

BARYON OSCILLATIONS AND CONSISTENCY TESTS FOR PHOTOMETRICALLY-DETERMINED REDSHIFTS OF VERY FAINT GALAXIES

HU ZHAN AND LLOYD KNOX

Department of Physics, University of California, Davis, CA 95616

Draft version July 3, 2019

ABSTRACT

Weak lensing surveys that can potentially place strong constraints on dark energy parameters can only do so if the source redshift means and error distributions are very well known. We investigate prospects for controlling errors in these quantities by exploiting their influence on the power spectra of the galaxies. Although, from the galaxy power spectra alone, sufficiently precise and simultaneous determination of redshift biases and variances is not possible, a strong consistency test is. Given the redshift error rms, galaxy power spectra can be used to determine the mean redshift of a group of galaxies to subpercent accuracy. Although galaxy power spectra cannot be used to determine the redshift error rms, they can be used to determine this rms divided by the Hubble parameter, a quantity that may be even more valuable for interpretation of cosmic shear data than the rms itself. We also show that galaxy power spectra, due to the baryonic acoustic oscillations, can potentially lead to constraints on dark energy that are competitive with those due to the cosmic shear power spectra from the same survey.

Subject headings: cosmological parameters — large-scale structure of universe — method:statistical

1. INTRODUCTION

Prospects of cosmic shear for cosmology (Hu 1999; Hu & Tegmark 1999; Hu 2002; Huterer 2002; Heavens 2003; Refregier 2003; Benabed & Van Waerbeke 2004; Ishak et al. 2004; Song & Knox 2004; Takada & Jain 2004; Takada & White 2004; Knox et al. 2005) have inspired many on-going and future weak lensing surveys such as the Deep Lens Survey¹, Canada France Hawaii Telescope Legacy Survey², and the Large Synoptic Survey Telescope³ (LSST, Tyson et al. 2003).

The statistical properties of cosmic shear maps depend on the distances to the lenses and sources. With the redshifts of the source galaxies determined, the data can thus be used to constrain dark energy parameters via their influence on the distance-redshift relation (Simpson & Bridle 2005; Knox, Song, & Tyson 2005). Because the source galaxies are faint and numerous their redshifts will be estimated from multi-band imaging data (photometric redshifts) rather than from spectroscopic data (spectroscopic redshifts). For redshift uncertainties not to degrade the constraints on dark energy parameters one must know the rms photometric redshift error and any biases very accurately (Bernstein & Jain 2004; Huterer et al. 2005; Ishak & Hirata 2005; Ma, Hu, & Huterer 2005).

Photometric redshifts are traditionally calibrated with spectroscopy of a subset of the imaged galaxies. One needs a very large and fair sample though in order to achieve a sufficiently accurate calibration. For example, to reduce the uncertainties of the rms photometric redshift error to 1%, a minimum of 5000 spectra are required in each redshift bin and ideally for each spectral type of galaxy. This is achievable at low redshift, but

it becomes prohibitively expensive toward high redshifts for the magnitude limits of the deepest planned surveys. Moreover, photometric redshift errors are not Gaussian; the distributions tend to have long tails. This means that the rms value may not be sufficient for characterizing photometric errors and that one needs an even larger spectroscopic subsample to map the full error distribution. Thus, it remains a challenge for very deep surveys to calibrate their photometric redshifts with sufficient accuracy.

However this challenge is met, we expect that independent cross checks capable of revealing inconsistencies with their nominal error distributions, will be very valuable. The clustering properties of galaxies in redshift space provide us with such an opportunity. Photometric redshift errors, like peculiar velocities, alter the galaxy power spectrum in redshift space. Specifically, they strongly suppress the power spectrum along the line of sight. The amount of suppression is exponentially sensitive to the rms photometric redshift error (e.g. Seo & Eisenstein 2003, hereafter SE03; Zhan et al. 2005). Thus, one can use the three-dimensional galaxy power spectrum to quantify photometric redshift errors and, consequently, prevent weak lensing statistics from severe degradation.

The clustering properties of the galaxies are also dark energy probes in their own right. The features in the galaxy power spectrum (the broadband shape and baryon acoustic oscillations) (Peebles & Yu 1970; Bond & Efstathiou 1984; Holtzman 1989; Hu & Sugiyama 1996; Cole et al. 2005; Eisenstein et al. 2005; Huetsi 2005) can be used as CMB-calibrated standard rulers for determining the angular-diameter distance $D(z)$ and constraining dark energy (Eisenstein, Hu, & Tegmark 1998; Blake & Glazebrook 2003; Hu & Haiman 2003; Linder 2003; SE03; Angulo et al. 2005).

Several papers have studied the prospects for measur-

Electronic address: zhan@physics.ucdavis.edu

Electronic address: lknox@physics.ucdavis.edu

¹ See <http://dls.physics.ucdavis.edu>.

² See <http://www.cfht.hawaii.edu/Science/CFHLS/>.

³ See <http://www.lsst.org>.

ing baryon acoustic oscillations from photometric surveys (SE03; Blake & Bridle 2004; Dolney, Jain, & Takada 2004; Glazebrook & Blake 2005; Linder 2005). The main advantage of a photometric redshift survey, is the wide coverage, which reduces the sample variance error, and deep photometry, which leads to more galaxies and therefore lower shot noise.

The challenges for large photometric redshift surveys include redshift errors, dust extinction, galaxy bias, redshift distortion and nonlinear evolution (Zhan et al. 2005). These non-idealities do not produce strong oscillating features in the power spectrum (similar to the baryon oscillations) and can be controlled, despite some degradation to the measurements (Seo & Eisenstein 2005; White 2005; Zhan et al. 2005).

Ideally, the clustering properties of the galaxies would be adequate to simultaneously constrain dark energy and the error distribution of the photometric redshift errors. As we show below though, such a self-calibration does not achieve a sufficiently accurate reconstruction of the photometric redshift error distribution. However, the clustering properties of the galaxies *can* provide a valuable, though somewhat model-dependent, consistency test.

In section 2 we present our method for forecasting constraints on cosmological parameters as well as parameters of the redshift error distribution. In Section 3 we show how well the rms photometric redshift error can be estimated given the knowledge of the Hubble parameter $H(z)$, and vice versa. We then demonstrate that mean redshifts can be accurately determined from the same data. In Section 4 we forecast constraints on dark energy from the broadband shape and baryon oscillations in the galaxies of the LSST survey. Since the constraints from the former alone are sub-dominant to those from the latter (SE03), hereafter we only refer to baryon oscillations even though the broadband shape is always included in our analysis. In Section 5 we discuss these results and conclude.

2. METHOD

SE03 developed a two-stage Fisher matrix analysis to forecast errors on dark energy equation of state (EOS) parameters from baryon oscillations. We adopt their method with improvements and constrain photometric redshift errors at the same time.

In the first stage of the SE03 analysis H_i and D_i , where $H_i \equiv H(z_i)$, $D_i \equiv D(z_i)$, and z_i is the mean redshift of the i th bin of galaxies, are treated as free parameters and their Fisher matrix is calculated. In the second stage, constraints on the matter density ω_m , the comoving angular diameter distance to the last scattering surface D_{CMB} , H_i and D_i are converted to constraints on dark energy parameters. The point of dividing the analysis into two stages is to allow one to better understand how the dark energy constraints are arising.

2.1. Observed Galaxy Power Spectrum

Using a fiducial cosmological model as reference, we can write the observed galaxy power spectrum as

$$P_g(k_{f\perp}, k_{f\parallel}) = \frac{D_f^2 H}{D^2 H_f} \left(1 + \beta \frac{k_{\parallel}^2}{k_{\perp}^2 + k_{\parallel}^2} \right)^2 \times |\tilde{W}(c^2 \sigma_z^2 k_{\parallel}^2 / H^2)|^2 b^2 G^2 P(k) + P_s, \quad (1)$$

where β is the linear redshift distortion parameter (Kaiser 1987), $\sigma_z = \sigma_{z0}(1+z)$ is the rms photometric redshift error, b is the galaxy clustering bias, G is the linear growth function, $P(k)$ is the matter power spectrum at $z=0$, and P_s is the shot noise. We have suppressed the argument z in functions D , D_f , H , H_f , β , σ_z , b , and G for convenience. The true wavenumbers k_{\perp} and k_{\parallel} are related to the fiducial ones by

$$k_{\perp} = k_{f\perp} D_f / D \text{ and } k_{\parallel} = k_{f\parallel} H / H_f. \quad (2)$$

The window function, \tilde{W} , in Eq. (1), is the Fourier transform in the radial direction of the real-space window function, W , which is the distribution of galaxies at true distance r given their estimated distance of \bar{r} . With the assumption that this distribution has the form

$$P(r|\bar{r}) = W((r - \bar{r}) / \sigma_r) \quad (3)$$

the modulus of the Fourier transform only depends on $k_{\parallel} \sigma_r = k_{\parallel} c \sigma_z / H$. If we further assumed a normal distribution then $|\tilde{W}|^2 = e^{-c^2 \sigma_z^2 k_{\parallel}^2 / H^2}$ and Eq. (1) would be the same as in SE03.

In all our calculations, for simplicity, we do assume a normal distribution for the redshift errors. But in general redshift errors are significantly non-Gaussian. Typically photometric redshift errors have long tails due to the fraction of redshift assignments that fail catastrophically. However, as can be seen from Eq. (1) any non-Gaussianity has its impact on the observed galaxy power spectrum and, in principle, by assuming the isotropy of $P(k)$, one can reconstruct the function \tilde{W} from the anisotropy of the observed galaxy power spectrum. Of course, with greater freedom allowed in the functional form of the redshift error distribution, the quality of the reconstruction will be weakened.

Scoccimarro (2004) points out that the Kaiser (1987) formula for the linear redshift distortion [used in Eq. (1)] may not be sufficiently accurate for the precision measurements we consider here. Fortunately, the effect of redshift distortion can be readily calibrated through N -body simulations. Meanwhile, one can also quantify the window function W by assigning realistic redshift errors to mock galaxies drawn from the simulations. Precisely calibrated matter power spectra are, in fact, required for interpreting weak lensing data (White 2004; Zhan & Knox 2004; Huterer & Takada 2005; Hagan, Ma, & Kravtsov 2005). As such, calibrating the effects of redshift distortion and photometric redshift errors can be achieved from the same set of simulations without much difficulty.

Although we treat them as constant across each redshift bin, all the functions (D , D_f , H , H_f , β , σ_z , b , and G) in equation (1), as well as the survey selection function, can change considerably within a single redshift bin. As such, the observed galaxy power spectrum in a redshift bin becomes a convolution of equation (1) with another window function that accounts for the radial evolution (e.g., as treated in Zhan et al. 2005). We avoid this complication for simplicity, although the appropriate treatment is straightforward as long as the true evolution within each bin is known, or can be parameterized.

The sub-bin evolution we are most concerned with is that of the clustering bias. The variation will be caused in part by any redshift dependence of the selection function. Even if one were selecting the same distribution of

galaxy types at each redshift, bias would change due to the intrinsic evolution of the population. Most importantly, redshift errors might actually be correlated with bias fluctuations since both can be caused by spectral type errors (Padmanabhan 2005). We do not yet know the magnitude of these effects and the extent to which they can be controlled.

2.2. Fisher Matrix

For the stage I analysis, our complete parameterization of the observables includes more than just H_i and D_i . There are four other parameters in each redshift bin: $\ln(G_i b_i)$, $\ln \beta_i$, $P_{s,i}$ and $\ln \sigma_{z,i}$, where i refers to the i th redshift bin, and seven redshift-independent parameters. We do not include the redshift bias parameters, δz_i , at this stage because they have no influence on the observed power spectra except through H_i and D_i , which are independent parameters in stage I. They will be included in stage II. For brevity, we suppress the subscript i in what follows.

The seven redshift-independent parameters are the matter density ω_m , the baryon density ω_b , the redshift of reionization z_{rei} , the primordial helium mass fraction y_p , the spectral tilt n_s , the normalization of the primordial potential power spectrum $k_0^3 P_{\Phi 0}$, and the angular size of the sound horizon at the last scattering surface θ_s .

There are three major difference between our choice of parameters and that of SE03. First, we do not include the matter fraction Ω_m because at fixed θ_s and ω_m it affects neither the CMB observables nor the matter power spectrum. Second, we use $\ln G b$ instead of $\ln G$ because the galaxy clustering bias is degenerate with the growth function. And third, we include additional parameters $\ln \sigma_z$ (stage I) and δz (stage II) in each redshift bin. We also replace D_{CMB} in SE03 with θ_s for convenience, which is not critical.

As the cosmic density field evolves, nonlinear effects become important on larger and larger scales. To prevent these effects from contaminating the measurements of baryon oscillations, we only use the Fourier modes at $k < k_{\text{max}}$ in our analysis, where k_{max} ranges from 0.12 to 0.53 $h \text{Mpc}^{-1}$ between $z = 0.31$ and 2.66 (see Table 1). Evidence from the 2-degree Field Galaxy Redshift Survey and the Sloan Digital Sky Survey suggests that the galaxy clustering bias at $z \sim 0.1$, despite some dependence on luminosity, is scale-independent on scales k less than a few tenths $h \text{Mpc}^{-1}$ (e.g. Verde et al. 2002; Tegmark et al. 2004). Hence, the upper bound in wavenumber also ensures that we can model the galaxy bias as a time-evolving but scale-independent quantity. For simplicity, our fiducial model has a bias $b(z) = 1 + 0.84z$ for all galaxies. It is straightforward to model the bias for each sub-sample of galaxies separately. In fact, it is beneficial to divide the galaxies into sub-samples, especially at low redshift where galaxy number density is high, because one can control photometric redshift errors much better for a homogeneous sample of galaxies (e.g. Padmanabhan et al. 2005).

We assume that the primordial potential power spectrum $k^3 P_{\Phi}^i(k) = k_0^3 P_{\Phi 0} (k/k_0)^{n_s-1}$. Our fiducial model is a low density and flat cold dark matter universe with a cosmological constant. It has $(\omega_m, \omega_b, z_{\text{rei}}, y_p, n_s, k_0^3 P_{\Phi 0}, \theta_s) = (0.146, 0.021, 6.3, 0.24, 1.0, 6.4 \times 10^{-11}, 0.60 \text{ deg})$ and the

reduced Hubble constant $h = 0.655$.

We calculate the Fisher matrix using the approximation (Tegmark 1997)

$$F_{ij} = \int \frac{1}{2} \frac{\partial \ln P(\mathbf{k}_f)}{\partial p_i} \frac{\partial \ln P(\mathbf{k}_f)}{\partial p_j} V_{\text{eff}}(\mathbf{k}_f) \frac{d\mathbf{k}_f}{(2\pi)^3}, \quad (4)$$

where p_i is the i th parameter,

$$V_{\text{eff}}(\mathbf{k}) = \int \left[\frac{n(\mathbf{r}) P_g(\mathbf{k})}{n(\mathbf{r}) P_g(\mathbf{k}) + 1} \right]^2 d\mathbf{r} \quad (5)$$

is the effective volume of the survey (Feldman et al. 1994), and $n(\mathbf{r})$ is the galaxy number density. The marginalized error of the i th parameter is given by $[(F + F_P)^{-1}]_{ii}^{1/2}$. Here, F_P is for any prior information. If we already know, prior to examining the data, the value of parameter p_i to within $\pm \sigma_P(p_i)$ then $(F_P)_{ii} = 1/\sigma_P^2(p_i)$.

In the second stage, our “observables” are ω_m , θ_s , D ’s, and H ’s with their covariance matrix as calculated from the stage I Fisher matrix, marginalizing over all the other parameters. From these observables, and their covariance matrix, we forecast how well one can determine the following parameters: the photometric redshift biases δz , ω_m , Ω_{DE} , w_0 , and w_a , where the dark energy EOS is parametrized as $w(z) = w_0 + w_a[1 - (1+z)^{-1}]$. To explicitly define the redshift bias parameters we write the probability that a galaxy with photometric redshift estimate z_p has a true redshift in between z and $z + dz$ as

$$dP(z) = \frac{1}{\sqrt{2\pi} \sigma_z} \exp \left[-\frac{(z + \delta z - z_p)^2}{2\sigma_z^2} \right] dz. \quad (6)$$

2.3. Tests

We test our procedures using the baseline surveys of SE03. In order to compare with their results, we do not include photometric redshift parameters and do not differentiate the photometric redshift term $e^{-c^2 \sigma_z^2 k_{\parallel}^2 / H^2}$ with respect to H in the Fisher matrix. We also adopt SE03 parametrization of the dark energy EOS in this test. The resulting uncertainties on D and H match those in SE03 within a factor of 1.2 (1.45) for the spectroscopic (photometric) baseline survey. Our error forecasts on dark energy parameters are 30%–50% larger than those in SE03 because of the larger errors we obtain for D and H .

If we include the derivative of the photometric redshift term $e^{-c^2 \sigma_z^2 k_{\parallel}^2 / H^2}$ with respect to H in the Fisher matrix, then the constraints on H and dark energy EOS parameters are nearly as good as those from the spectroscopic baseline survey. This is because the shape of the observed galaxy power spectrum is exponentially sensitive to the Hubble parameter. Such sensitivity imposes a strong constraint on H and subsequently on dark energy EOS parameters. However, the strong constraint is actually on the comoving length scale of the rms photometric redshift error $c\sigma_z/H$. In reality, the uncertainty of σ_z will degrade the constraint on H . In fact, if we also include $\ln \sigma_z$ in the parameter set, the constraints become as weak as those from the photometric baseline survey in the previous paragraph. Thus, we conclude that the photometric results in SE03 are equivalent to having an imprecise prior on σ_z ; i.e., letting σ_z float freely.

TABLE 1
MARGINALIZED ERRORS OF SELECTED STAGE I PARAMETERS
WITH COMPLETE SELF-CALIBRATION FROM LSST

z	k_{\max} ($h \text{ Mpc}^{-1}$)	$\sigma(\ln D)^a$	$\sigma(\ln H)^a$	$\sigma(\ln H)^b$	$\sigma(\ln \sigma_z/H)^{a,c}$ ($\times 100$)	$\sigma(\ln \beta)^a$	$\sigma(\ln Gb)^a$
0.31	0.12	2.9	27	1.1	0.37	24	13
0.55	0.14	1.7	19	1.0	0.21	17	9.5
0.84	0.17	0.75	14	1.0	0.14	13	7.1
1.18	0.21	0.57	12	1.0	0.11	11	6.2
1.59	0.28	0.43	10	1.0	0.10	9.4	5.2
2.08	0.38	0.39	11	1.0	0.11	10	5.5
2.66	0.53	0.43	12	1.0	0.15	13	6.4

^a No prior is taken for the rms photometric redshift error or the Hubble parameter. The constraints are poorer at low redshift due to small volumes and low k_{\max} and then are poorer at high redshift due to low galaxy number densities.

^b We assume $\sigma_P(\ln \sigma_z) = 0.01$ for this column. The prior sets the precision of H , reduces uncertainties of β and Gb significantly, and renders little improvement to other parameters.

^c For this column, the parameter $\ln \sigma_z$ in the Fisher matrix is replaced by $\ln \sigma_z/H$. With this parametrization, the constraints on other parameters change slightly.

3. RESULTS FOR REDSHIFT PARAMETERS

We assume that through some external calibration process we have estimates of both the distribution of errors about the mean redshift as well as the mean redshift. A central point of our paper is that one can use the clustering properties of the galaxies themselves to test these externally-derived mean redshifts. To explain how it works, let us assume that the distribution of errors is Gaussian with variance σ_z^2 . The redshift errors lead to a suppression of the fluctuation power of radial modes by an amount $\exp(-c^2 \sigma_z^2 k_{\parallel}^2 / H^2)$. With σ_z known, one can thus determine H . Analyzing the power spectra of a sequence of galaxy groupings, each with mean redshifts, z_m , we thus know $H(z_m - \delta z)$ for each group of galaxies. From the standard ruler provided by the baryon oscillations, we can also determine $D(z_m - \delta z)$. With some assumptions about the smoothness of H , and using the fact that $D = c \int dz/H$, these values of D and H will not be consistent with each other for all possible values of $z_m - \delta z$. Thus we can determine these mean redshifts and check to see if they are consistent with the mean redshifts inferred from the external calibration.

Even if we do not use the external calibration to tell us σ_z , from the galaxy power spectra we can still determine the source distance rms $\sigma_r = c\sigma_z/H$ to much better than 1% (see Table 1). Fortunately, this is exactly the quantity we want for interpretation of weak lensing power spectra, since the weak lensing power spectrum for sources with mean redshift z depends on how the sources are distributed in real space, not redshift space.

In this section we investigate quantitatively how well one can measure σ_z , given H (and vice-versa), perform the redshift bias consistency test and determine σ_z/H . For specificity, we adopt for this section and the next a model of the proposed survey by LSST as our fiducial survey. We assume a survey area of 23,000 square degrees with galaxy distribution

$$n(z) = 640z^2 e^{-z/0.35} \text{ arcmin}^{-2}, \quad (7)$$

which corresponds to a projected number density of 55 arcmin^{-2} . We use $\sigma_{z0} = 0.04$ as our fiducial rms photometric redshift error. The survey is divided into 7 redshift bins from $z = 0.2$ to 3 each with roughly the same

comoving radial extent. The mean redshifts of the redshift bins are listed in Table 1.

For the CMB we assume *Planck* as treated in Kaplinghat, Knox, & Song (2003). *Planck* observes at 9 different frequency channels from 30 to 850 GHz. To crudely model the effects of foregrounds we assume the temperature maps at 100, 143 and 217 GHz can be perfectly cleaned of foregrounds by use of the other channels and for polarization we keep just the 143 and 217 GHz channels. We assume this can be done over 80% of the sky up to $l_{\max} = 2000$ for temperature and $l_{\max} = 2500$ for polarization.

3.1. rms Photometric Redshift Error and H

We first implement the full procedure described in Section § 2 with a prior on the Hubble parameter $\sigma_P(\ln H)$. For a simple demonstration, we apply the same prior to all redshift bins. The results for four of the redshift bins are shown in Fig. 1. The other three are suppressed for clarity. As expected, the prior on H sets directly the uncertainty of the rms photometric redshift error, i.e. $\sigma(\ln \sigma_z) = \sigma_P(\ln H)$, over a wide range. One is limited by the uncertainty of the combination σ_z/H when the prior $\sigma_P(\ln H)$ is stronger than the constraint $\sigma[\ln(\sigma_z/H)]$, so that $\sigma_P(\ln H)$ can no longer improve the precision of σ_z . On the other hand, $\sigma(\ln \sigma_z)$ does not degrade further when the prior is worse than what can be determined from the survey itself. Hence, the $\sigma(\ln \sigma_z) - \sigma_P(\ln H)$ curves in Fig. 1 flatten on both sides.

A prior on the Hubble parameter could potentially come from a spectroscopic galaxy survey such as that planned with the Kilo-Aperture Optical Spectrograph⁴. KAOS will be able to survey enough volume to determine the Hubble parameter at $z \sim 1$ and 3 to a few percent from baryon oscillations (SE03).

On the other hand, we may take a prior on σ_z from a spectroscopic calibration of the photometric redshifts. We have thus also calculated the effect of a prior on the rms photometric redshift error $\sigma_P(\ln \sigma_z)$ on our ability to determine H . Again, the same prior was taken for the seven redshift bins. The results are almost identical to

⁴ See <http://www.noao.edu/kaos/>.

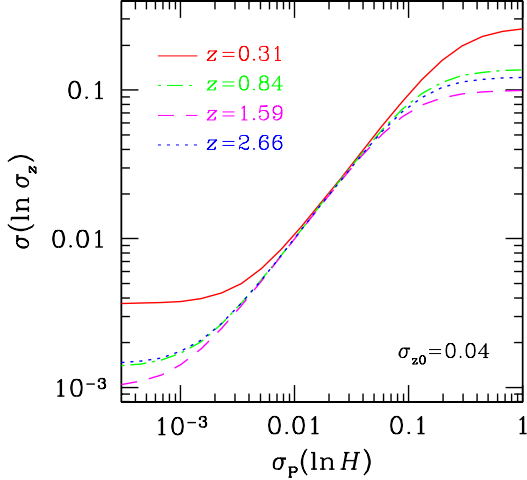


FIG. 1.— Fractional errors on the rms photometric redshift error $\sigma(\ln \sigma_z)$ as a function of the prior on the Hubble parameter $\sigma_P(\ln H)$ in four of the seven redshift bins assuming the fiducial LSST survey. On the left side, the prior is better than the constraint of the combination σ_z/H (see Table 1), so that it can no longer improve the precision of σ_z . Whereas, on the right side, the prior is not useful because the survey constrains H better than the prior, i.e. it reaches self-calibration. In the middle, one has $\sigma(\ln \sigma_z) = \sigma_P(\ln H)$ as expected. The uncertainty of H as a function of the prior on σ_z look identical to this figure except the x-axis label becomes $\sigma_P(\ln \sigma_z)$ and the y-axis label $\sigma(\ln H)$.

those in Fig. 1 but with x-axis label becoming $\sigma_P(\ln \sigma_z)$ and the y-axis label $\sigma(\ln H)$, because σ_z and H are degenerate in the photometric suppression $e^{-c^2 \sigma_z^2 k_{\parallel}^2 / H^2}$.

3.2. Photometric Redshift Bias

In stage II of the Fisher matrix analysis, we include redshift biases δz . These redshift biases will cause inconsistencies between the angular diameter distance and Hubble parameter in a given cosmological model, given some assumptions about the smoothness of H . In our analysis, those smoothness assumptions are provided implicitly by modeling the dark energy density as a smoothly varying function, controlled by EOS parameters w_0 and w_a .

The resulting constraints on the photometric redshift biases are shown in Fig. 2 as a function of the input prior $\sigma_P(\ln \sigma_z)$, which is the same in all redshift bins. With $\sigma_P(\ln \sigma_z) \sim 0.01$ the biases are determined to better than 0.01. For the 4,000 sq. degree cosmic shear survey considered by Ma et al. (2005), these bias constraints are sufficient to keep the degradation in w_0 and w_a errors at the 20% and 50% levels respectively. However, because the larger LSST cosmic shear survey can achieve stronger constraints on w_0 and w_a (given perfect redshift information), the degradation in w_0 and w_a in this case is worse: factors of 2.5 and 3 respectively⁵. This degradation is much better though than the factor of 10 degradation in w_0 and w_a that occur without any prior on the redshift biases.

At low $\sigma_P(\ln \sigma_z)$ the quality of the constraint as a function of z peaks at intermediate redshifts, due to the similar behavior for the constraints on D and H (see Table 1).

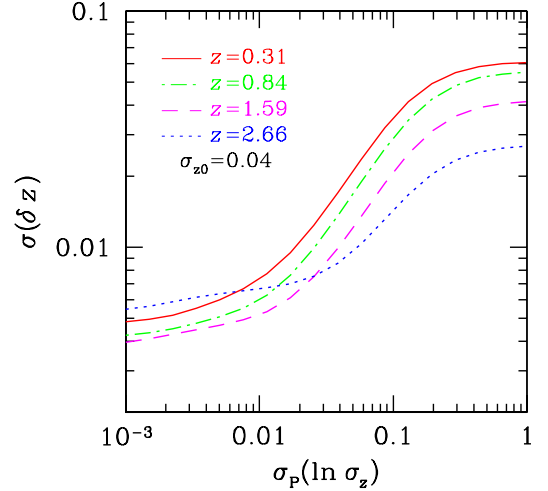


FIG. 2.— Forecasted errors on δz given varying priors on σ_z . At low $\sigma_P(\ln \sigma_z)$ the quality of the constraint as a function of z peaks at intermediate redshifts, due to the similar behavior for the constraints on D and H (see Table 1).

4. DARK ENERGY CONSTRAINTS FROM LSST BARYON ACOUSTIC OSCILLATIONS

While the constraints on σ_z and δz from galaxy power spectra discussed in Section 3 will be useful for extracting dark energy constraints from cosmic shear data, we also explore how well dark energy information can be extracted from the galaxy power spectra themselves.

In Figures 3 and 4 we see contours of constant forecasted errors in w_0 and w_a as the redshift priors are varied. The same priors are applied to all redshift bins for simplicity. As expected, the galaxy power spectrum alone provides for only a very weak self-calibration; as the prior on rms redshift errors is relaxed to 100% and that on redshift biases to 0.1, the errors degrade by factors of 20 to 40. Also as expected, we do see though that with a strong prior on σ_z , one does not need a prior on the δz parameters.

From Fisher matrix calculations like those in Section 3 we find that the Hubble parameter does not significantly improve the constraints on dark energy EOS parameters unless it is determined with precision comparable to or better than those of the angular diameter distance. This means that one must achieve $\sigma(\ln H) \lesssim 1\%$, which is possible, as discussed in Section 3.1, with a prior of $\sigma_P(\ln \sigma_z) \lesssim 1\%$.

We show LSST baryon oscillation constraints on w_0 and w_a in Fig. 5 for two cases: $[\sigma_z, \sigma_P(\ln \sigma_z), \sigma_P(\delta z)] = (0.04, 0.01, 0.01)$ (dashed line) and $(0.08, 0.005, 0.08)$ (solid line). By reducing $\sigma_P(\ln \sigma_z)$ from 0.01 to 0.005 one tightens the constraints considerably, even though the rms photometric redshift error is increased. This example demonstrates that a large rms photometric redshift error can be tolerated as long as it is known accurately.

We also show in Fig. 5 the constraints from the power spectra of LSST tomographic cosmic shear maps (dotted line) and 2000 supernovae as might be observed by the Joint Dark Energy Mission (dash-dotted line, Knox, Albrecht, & Song 2005). Note that these weak lensing error forecasts are done in the limit of perfect prior knowledge of the redshift error distribution param-

⁵ Zhaoming Ma, private communication.

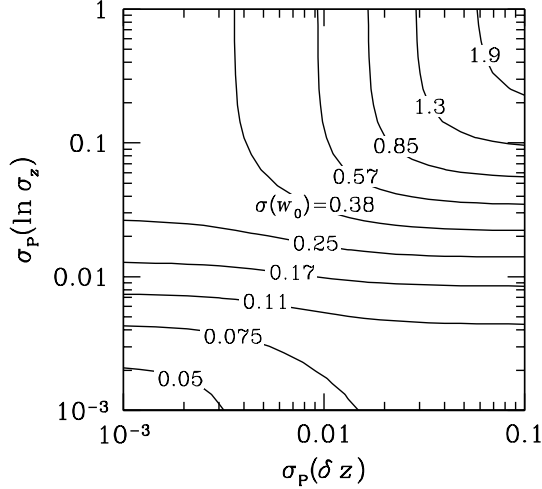


FIG. 3.— Contours of constant forecasted errors in w_0 estimated from galaxy clustering in the LSST survey as priors on δz and σ_z are varied. The same priors are applied to all redshift bins for simplicity.

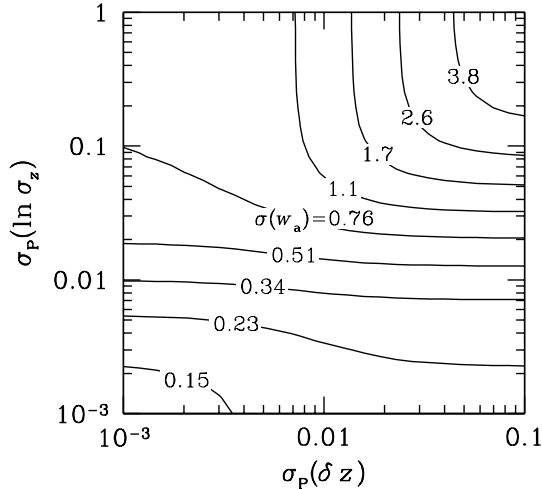


FIG. 4.— As in Fig. 3, but the contours are for constant error in w_a .

eters. If we were to use the priors on these parameters adopted for the baryon oscillation calculations, the weak lensing constraints would become slightly looser than the baryon oscillation constraints.

One may attempt to combine all the three constraints together to achieve higher precision. However, further work is needed to carefully account for the correlation between baryon oscillations and weak lensing statistics, because they overlap in both observational data and underlying density field (e.g. Hu & Jain 2004).

As mentioned earlier, we cannot yet be completely sure that the sub-bin evolution of galaxy bias can be controlled well enough to make an accurate determination of $\tilde{W}(c\sigma_z k_{\parallel}/H)$, the suppression of power in the radial direction. If we are not able to extract the information about the shape of the window function and, therefore, σ_z/H , then even with a prior on the redshift error distribution from external calibration our determination of $H(z)$ will be degraded as discussed in Section 3.1. We show in Fig. 6 how the error contours degrade in the

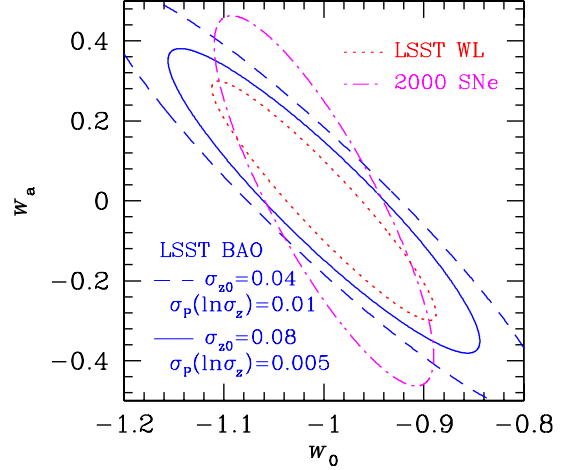


FIG. 5.— Marginalized 1σ error contours in the w_0 - w_a plane. The contours for LSST baryon acoustic oscillations are shown for $[\sigma_z, \sigma_P(\ln \sigma_z), \sigma_P(\delta z)] = (0.04, 0.01, 0.01)$ (dashed line) and $(0.08, 0.005, 0.08)$ (solid line). For comparison, we include the error ellipses from the power spectra of LSST tomographic cosmic shear maps (dotted line) and 2000 supernovae as might be observed by the Joint Dark Energy Mission (dash-dotted line, Knox et al. 2005). Note that the weak lensing constraints, unlike the baryon oscillation constraints, do not include the effects of redshift error distribution uncertainties.

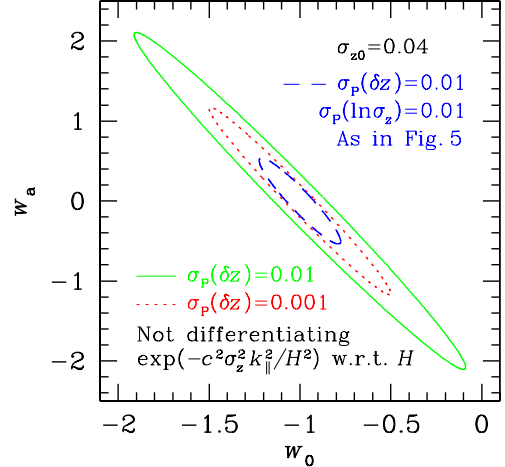


FIG. 6.— As in Fig. 5, but the two larger error contours are obtained without differentiating the photometric suppression term $\exp(-c^2 \sigma_z^2 k_{\parallel}^2 / H^2)$ with respect to the Hubble parameter H in the Fisher matrix in stage I. The rms photometric redshift error is assumed to be $\sigma_z = 0.04(1+z)$, and it is not included as parameters. In stage II, the same prior is applied to the photometric redshift bias in each redshift bin. The solid contour corresponds to $\sigma_P(\delta z) = 0.01$, and the dotted contour $\sigma_P(\delta z) = 0.001$. The constraints do not improve for $\sigma_P(\delta z) \lesssim 0.001$ or degrade much for $\sigma_P(\delta z) \gtrsim 0.008$. The dashed contour is from Fig. 5 for $[\sigma_z, \sigma_P(\ln \sigma_z), \sigma_P(\delta z)] = (0.04, 0.01, 0.01)$.

limit of no information extracted from the shape of the radial suppression. Specifically, for this calculation we do not differentiate the photometric suppression term $e^{-c^2 \sigma_z^2 k_{\parallel}^2 / H^2}$ with respect to H in stage I, and the parameters $\ln \sigma_z$ are removed. In other words, this is the calculation in the SE03 limit as discussed earlier. Unlike in SE03 we include photometric redshift biases δz in stage II to explore their effect on dark energy constraints. The error contour with $[\sigma_z, \sigma_P(\ln \sigma_z), \sigma_P(\delta z)] = (0.04, 0.01, 0.01)$

(dashed line) from Fig. 5 is added for comparison.

One sees in Fig. 6 that the constraints from baryon oscillations in photometric redshift surveys are tightened tremendously by fully utilizing our knowledge of the photometric suppression to the galaxy power spectrum. Without extracting information from $e^{-c^2\sigma_z^2 k_{\parallel}^2/H^2}$, we obtain $[\sigma(\Omega_{\text{DE}}), \sigma(w_0), \sigma(w_a)] = (0.046, 0.33, 0.77)$ for $\sigma_{\text{P}}(\delta z) = 0.001$ (dotted line) and $(0.084, 0.60, 1.4)$ for $\sigma_{\text{P}}(\delta z) = 0.01$ (solid line). These constraints are as loose as those with very weak priors on $\ln \sigma_z$ in Figs. 3 and 4. They do not improve for $\sigma_{\text{P}}(\delta z) \lesssim 0.001$ or degrade much for $\sigma_{\text{P}}(\delta z) \gtrsim 0.008$.

5. DISCUSSION AND CONCLUSIONS

The statistical properties of weak lensing maps are sensitive to the distances to the sources, and not to the redshifts of the sources. Therefore, even without redshift information, weak lensing observations can be used to determine the source distance distribution. The redshift information is needed only so the source distance distribution can inform us about the distance-redshift relation. However, this distance-redshift relation is exactly what we want, because of its sensitivity to dark energy, and therefore the redshift information is actually terribly important.

We have pointed out that the three-dimensional power spectra of the source galaxies, because of their sensitivity to redshift errors, can be used to inform us about the source redshift distribution. While the galaxy power spectra, on their own, cannot give us all we need to know for interpretation of tomographic cosmic shear data, they can be used to *supplement* the redshift information available from external calibration of the photometric redshifts.

We have demonstrated the supplemental information available in two different ways. First, if one uses prior information (perhaps from external calibration) about the variance of the redshift errors in each of the redshift bins, then the mean redshifts of each of those redshift bins can be recovered. They can be recovered with sufficient precision to greatly limit the degradation in the errors on

dark energy EOS parameters reconstructed from cosmic shear data. Second, without any prior on the redshift error variance, the three-dimensional galaxy power spectra can be used to determine very precisely the source distance distribution which with the assumption of a normal distribution is specified by the combination σ_z/H . The source distance distribution will be very helpful for interpretation of cosmic shear data. Although, for determining the distance-redshift relation (and thereby the dark energy EOS parameters) we will still require mean redshifts for each of the redshift bins, in this case from some external calibration.

The galaxy power spectra, combined with external calibration of the source redshift distributions, are also potentially powerful probes of dark energy. *If* the rms photometric redshift error is determined to better than 1% through some external calibration of an unbiased subsample, and one can control sub redshift bin bias evolution then one can significantly reduce errors on the Hubble parameter and, consequently, put tight constraints on the dark energy EOS parameters using baryon acoustic oscillations. For instance, with priors $\sigma_{\text{P}}(\ln \sigma_z) = 0.005$ and $\sigma_{\text{P}}(\delta z) \lesssim 0.004$, one can achieve $\sigma(\Omega_{\text{DE}}) = 0.015$, $\sigma(w_0) = 0.095$, and $\sigma(w_a) = 0.24$ with LSST.

Achieving, in practice, the constraints on dark energy from baryon oscillations and cosmic shear, that are possible in principle, will require very accurate calibrations of photometric redshifts for very faint galaxies. This is a significant challenge for the observational community. The consistency tests we have described here may play an important role in meeting that challenge.

We thank Y. S. Song for providing the CMB Fisher matrix. We thank D. Eisenstein, Z. Ma, N. Padmanabhan, and J. A. Tyson for useful conversations and McGill University for their hospitality while some of this work was completed. This work was supported by the National Science Foundation under Grant No. 0307961 and NASA under grant No. NAG5-11098.

REFERENCES

- Alcock, C. & Paczynski, B. 1979, *Nature*, 281, 358
 Angulo, R., Baugh, C. M., Frenk, C. S., Bower, R. G., Jenkins, A., & Morris, S. L. 2005, *MNRAS* in press (astro-ph/0504456)
 Benabed, K., & Van Waerbeke, L. 2004, *Phys. Rev. D*, 70, 123515
 Bernstein, G., & Jain, B. 2004, *ApJ*, 600, 17
 Blake, C. & Bridle, S. 2004, submitted to *MNRAS* (astro-ph/0411713)
 Blake, C. & Glazebrook, K. 2003, *ApJ*, 594, 665
 Bond, J. R. & Efstathiou, G. 1984, *ApJ*, 285, L45
 Cole, S. et al. 2005, submitted to *MNRAS* (astro-ph/0501174)
 Dolney, D., Jain, B., & Takada, M. 2004, *ArXiv Astrophysics e-prints* (astro-ph/0409445)
 Eisenstein, D. J., Hu, W., & Tegmark, M. 1998, *ApJ*, 504, L57
 Eisenstein, D. J. et al. 2005, submitted to *ApJ* (astro-ph/0501171)
 Feldman, H. A., Kaiser, N., & Peacock, J. A. 1994, *ApJ*, 426, 23
 Glazebrook, K. & Blake, C. 2005, *ApJ* in press, (astro-ph/0505608)
 Hagan, B., Ma, C.-P., & Kravtsov, A. V. 2005, *ApJ* in press (astro-ph/0504557)
 Heavens, A. 2003, *MNRAS*, 343, 1327
 Holtzman, J. A. 1989, *ApJS*, 71, 1
 Hu, W. 1999, *ApJ*, 522, L21
 Hu, W. 2002, *Phys. Rev. D*, 66, 083515
 Hu, W. & Haiman, Z. 2003, *Phys. Rev. D*, 68, 063004
 Hu, W. & Jain, B. 2004, *Phys. Rev. D*, 70, 043009
 Hu, W. & Sugiyama, N. 1996, *ApJ*, 471, 542
 Hu, W., & Tegmark, M. 1999, *ApJ*, 514, L65
 Huetsi, G. 2005, submitted to *A&A* (astro-ph/0507678)
 Huterer, D. 2002, *Phys. Rev. D*, 65, 063001
 Huterer, D., & Takada, M. 2005, *Astroparticle Phys.*, 23, 369
 Huterer, D., Takada, M., Bernstein, G., & Jain, B. 2005, submitted to *MNRAS* (astro-ph/0506030)
 Ishak, M., & Hirata, C. M. 2005, *Phys. Rev. D*, 71, 023002
 Ishak, M., Hirata, C. M., McDonald, P., & Seljak, U. 2004, *Phys. Rev. D*, 69, 083514
 Kaiser, N. 1987, *MNRAS*, 227, 1
 Kaplinghat, M., Knox, L., & Song, Y. S. 2003, *Phys. Rev. Lett.*, 91, 241301
 Knox, L. 2005, submitted to *Phys. Rev. D* (astro-ph/0503405)
 Knox, L., Albrecht, A., & Song, Y. S. 2005, *ASP Conf. Ser.* 339: *Observing Dark Energy*, 107
 Knox, L., Song, Y. S., & Tyson, J. A. 2005, submitted to *Phys. Rev. Lett.* (astro-ph/0503644)
 Linder, E. V. 2003, *Phys. Rev. D*, 68, 083504
 Linder, E. V. 2005, *ArXiv Astrophysics e-prints* (astro-ph/0507308)
 Ma, Z., Hu, W., & Huterer, D. 2005, submitted to *ApJ* (astro-ph/0506614)
 Padmanabhan, N. 2005, private communication
 Padmanabhan, N. et al. 2005, *MNRAS*, 359, 237
 Peebles, P. J. E. & Yu, J. T. 1970, *ApJ*, 162, 815

- Refregier, A. 2003, ARA&A, 41, 645
Scoccimarro, R. 2004, Phys. Rev. D, 70, 083007
Seo, H. & Eisenstein, D. J. 2003, ApJ, 598, 720
Seo, H. & Eisenstein, D. J. 2005, ApJ in press (astro-ph/0507338)
Simpson, F., & Bridle, S. 2005, Phys. Rev. D, 71, 083501
Song, Y. & Knox, L. 2004, Phys. Rev. D, 70, 063510
Takada, M., & Jain, B. 2004, MNRAS, 348, 897
Takada, M., & White, M. 2004, ApJ, 601, 1
Tegmark, M. 1997, Physical Review Letters, 79, 3806
Tegmark, M. et al. 2004, ApJ, 606, 702
Tyson, J. A., Wittman, D. M., Hennawi, J. F., & Spergel, D. N. 2003, Nuclear Physics B, Proceedings Supplements, 124, 21
Verde, L. 2002, MNRAS, 335, 432
White, M. 2004, Astroparticle Phys., 22, 211
White, M. 2005, ArXiv Astrophysics e-prints (astro-ph/0507307)
Zhan, H., & Knox, L. 2004, ApJ, 616, L75
Zhan, H., Knox, L., Tyson, J. A., & Margoniner V. 2005, submitted to ApJ (astro-ph/0508119)